Journal of Hazardous Materials 196 (2011) 36–43

Contents lists available at SciVerse ScienceDirect

Journal of Hazardous Materials

journal homepage: www.elsevier.com/locate/jhazmat

Thiol-functionalization of metal-organic framework by a facile coordination-based postsynthetic strategy and enhanced removal of Hg^{2+} from water

Fei Ke [a], Ling-Guang Qiu [a,*], Yu-Peng Yuan [a], Fu-Min Peng [a], Xia Jiang [a], An-Jian Xie [a], Yu-Hua Shen [a], Jun-Fa Zhu [b]

[a] Laboratory of Advanced Porous Materials, School of Chemistry and Chemical Engineering, Anhui University, Hefei 230039, China
[b] National Synchrotron Radiation Laboratory, University of Science and Technology of China, Hefei 230029, China

ARTICLE INFO

Article history:
Received 22 June 2011
Received in revised form 8 August 2011
Accepted 26 August 2011
Available online 3 September 2011

Keywords:
Metal-organic frameworks
Functionalization
Coordinatively unsaturated metal centers
Postsynthetic strategy
Heavy metal removal

ABSTRACT

The presence of coordinatively unsaturated metal centers in metal-organic frameworks (MOFs) provides an accessible way to selectively functionalize MOFs through coordination bonds. In this work, we describe thiol-functionalization of MOFs by choosing a well known three-dimensional (3D) Cu-based MOF, i.e. $[Cu_3(BTC)_2(H_2O)_3]_n$ (HKUST-1, BTC = benzene-1,3,5-tricarboxylate), by a facile coordination-based postsynthetic strategy, and demonstrate their application for removal of heavy metal ion from water. A series of $[Cu_3(BTC)_2]_n$ samples stoichiometrically decorated with thiol groups has been prepared through coordination bonding of coordinatively unsaturated metal centers in HKUST-1 with –SH group in dithioglycol. The obtained thiol-functionalized samples were characterized by powder X-ray diffraction, scanning electron microscope, energy dispersive X-ray spectroscopy, infrared spectroscopy, and N_2 sorption–desorption isothermal. Significantly, the thiol-functionalized $[Cu_3(BTC)_2]_n$ exhibited remarkably high adsorption affinity ($K_d = 4.73 \times 10^5$ mL g^{-1}) and high adsorption capacity (714.29 mg g^{-1}) for Hg^{2+} adsorption from water, while the unfunctionalized HKUST-1 showed no adsorption of Hg^{2+} under the same condition.

1. Introduction

Heavy metals released into the environment have posed a significant threat to the environment and public health due to the fact that they can accumulate in the human body [1,2]. As a result, the removal and recovery of heavy metal ions from industrial waste water have been a significant concern in most industrial branches. A number of technologies, such as chemical precipitation [3], adsorption [4], membrane systems [5], ionic exchange [6], and liquid extraction [7], have been developed over the years, among them adsorption technology has attracted considerable attention due to its simplicity and low cost. Many kinds of adsorbents, such as activated carbon, coal fly ash and zeolites, have been used for the removal of heavy metal ions from wastewater [8–10]. Recently, mesoporous silicas modified by functional groups such as $–NH_2$ and –SH have been demonstrated to be a new type of high-efficient heavy metal adsorbent. These silica-based adsorbents have unique large specific surface areas and regular pore structures. Significantly, the functional groups modified on the pore surface of adsorbents afford these materials the ability to interact strongly with metallic cations [11]. A variety of amino- or thiol-functionalized mesoporous silica materials have been successfully fabricated. However, the synthesis procedure of these functionalized mesoporous silica is considerably complicated. Large amounts of surfactants have to be used as a structure-directing agent. To remove surfactant molecules from pores formed in the solid, the sample obtained has to be extracted several times using a large amount organic of solvent or calcined in air at a high temperature.

Porous metal-organic frameworks (MOFs) [12], a new kind of crystalline porous material formed by metal ions (or clusters) and multidentate organic ligands, have been currently of intensively attraction, due to their great potential applications in catalysis [13,14] separations [15], drug delivery [16–19], gas storage [20], and sensing [21]. Their porous structures provide apparent surface areas of up to 5200 m^2 g^{-1} [22], together with a large variety of pore dimensions and topologies. Remarkably, the ability to chemically modulate the physicochemical properties of MOF structures after

* Corresponding author. Tel.: +86 551 5108212; fax: +86 551 5108212.
E-mail addresses: lgqiu@ahu.edu.cn, lgahu@163.com (L.-G. Qiu).

0304-3894/$ – see front matter © 2011 Elsevier B.V. All rights reserved.
doi:10.1016/j.jhazmat.2011.08.069

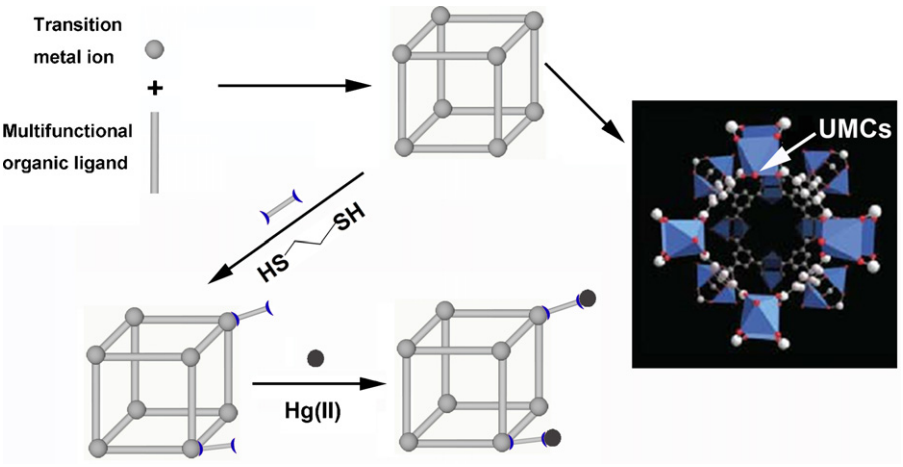

Fig. 1. Schematic illustration of the thiol-functionalization of MOFs through coordination bonding between one thiol group of dithioglycol and coordinatively unsaturated metal centers (UMCs) in MOFs.

the formation of crystalline MOFs by a postsynthetic modification (PSM) concept allows tuning of the interactions with guest species, and increases the use of MOFs as high performance, tailor-made materials [23].

There are mainly three different strategies to achieve MOF functionalization by PSM strategies. The first relies on non-covalent interactions include guest removal, guest exchange, or ion exchange [24,25], whereas the second approach exploits functional properties by the covalent modification of porous MOFs [26,27]. The presence of coordinatively unsaturated metal centers (UMCs) in MOFs materials also provides functionalization of MOFs, and the resulting functionalized MOFs have clearly demonstrated to exhibit highly selective separation, chemisorptions, and catalytic performance [28–31].

Herein we describe the synthesis of thiol-functionalized MOFs by a facile coordination-based PSM strategy (see Fig. 1) and their application for Hg^{2+} adsorption. To demonstrate such PSM route to thiol-functionalized MOFs, we chose a well known copper-based MOF with UMCs, $[Cu_3(BTC)_2(H_2O)_3]_n$ (HKUST-1, BTC = benzene-1,3,5-tricarboxylate) [32]. HKUST-1 has a three dimensional (3D) square-shaped channel system (9 × 9 Å) that contains up to 10 additional water molecules per formula unit. The lability of axial aqua ligands on the paddle-wheel secondary building units in $[Cu_3(BTC)_2(H_2O)_3]_n$ permits their replacement by other molecules. The coordinated water molecules in the framework as well as excess of water guests in the channels can easily be removed after vacuum treatment at 150 °C for 12 h, thus providing accessible sites for the surface functionalization. By treating the dehydrated MOF with dithioglycol, a series of thiol-functionalized MOF-based materials has been prepared. Their application for removal of heavy metal ions was preliminarily demonstrated by Hg^{2+} adsorption from water. Significantly, the resulting thiol-functionalized MOF exhibited both high adsorption affinity ($K_d = 4.73 \times 10^5$ mL g^{-1}) and remarkable adsorption capacity (714.29 mg g^{-1}) for Hg^{2+} adsorption from water, clearly demonstrating that thiol-functionalized MOFs could act as useful and effective adsorbents to remove heavy metal ions from the contaminated water.

2. Experimental

2.1. Materials and methods

Benzene-1,3,5-tricarboxylic acid (H_3BTC) was purchased from Aldrich, cupric nitrate trihydrate was purchased from Sinopharm (Shanghai) Chemical Reagent Co., Ltd., China, and dithioglycol was purchased from Tokyo Chemical Industry Co., Ltd., Japan. All other chemicals used in this work were of analytical grade, obtained from commercial suppliers, and used without further purification unless otherwise noted. High concentration (1431.04 mg L^{-1}) Hg^{2+} solution used for adsorption experiments, as well as Hg^{2+} stock solutions (6.51 mg L^{-1}), were prepared by dissolving irradiated $HgCl_2$ in deionized water, while Hg^{2+} solutions at lower concentrations (0.081–1.30 mg L^{-1}) were prepared by dilution of measured volumes of stock solution (6.51 mg L^{-1}) with deionized water.

The powder X-ray diffraction (PXRD) patterns of the samples were collected using an X-ray diffractometer with Cu target (36 kV, 25 mA) from 5 to 50°. Hg contents were determined by atomic fluorescence spectrometry (AFS) using a AFS-3100 spectrometer. Analyses of the morphology and chemical composition of the samples were conducted by a Hitachi S-4800 field emission scanning electron microscope (FE-SEM) equipped with an energy dispersive X-ray (Oxford Instruments INCA EDX) system. Nitrogen sorption–desorption isotherms were obtained at 77 K on a Micromeritics ASAP 2020M+C analyzer.

2.2. Synthesis of thiol-functionalized $[Cu_3(BTC)_2]_n$ samples

$[Cu_3(BTC)_2(H_2O)_3]_n$ crystals were prepared by a solvothermal reaction as reported previously [32]. Typically, 1.087 g (4.5 mmol) of $Cu(NO_3)_2{\cdot}3H_2O$ was dissolved in 15 mL deionized water and then mixed with 0.525 g (2.5 mmol) of H_3BTC dissolved in 15 mL ethanol. The mixture was stirred for 30 min, and then transferred to a 50 mL Teflon autoclave liner and sealed to heat at 120 °C for 12 h. The obtained blue powder was filtered off, washed several times with deionized water and ethanol, and then dried overnight at 150 °C under air atmosphere. Yield of $[Cu_3(BTC)_2(H_2O)_3]_n$ crystals was calculated to be 65.04% on the basis of Cu.

To prepare the thiol-functionalized $[Cu_3(BTC)_2]_n$ samples, 0.1 g as-synthesized $[Cu_3(BTC)_2(H_2O)_3]_n$ sample was dehydrated at 150 °C for 12 h, and then suspended in 10 mL of anhydrous toluene. An appropriate amount of 0.24 mol L^{-1} dithioglycol solution (0.5 mL for sample **A**, 1 mL for **B**, and 1.5 mL for **C**, respectively) in anhydrous toluene was added to the suspension, and the mixture solution was then stirred magnetically for 24 h at room temperature. The product was recovered by filtration and washed with ethanol (15 mL × 5), and then dried overnight at room temperature in vacuum. The relative contents of S in the functionalized samples **A**, **B** and **C** were determined by EDX spectra. The molar ratios of S to Cu in the framework for samples **A**, **B** and **C** were calculated to be 0.18, 0.92, 1.52, respectively, and thus the obtained

samples **A**, **B**, and **C** were also labeled as Cu-BTC-DTG-0.18, Cu-BTC-DTG-0.92, and Cu-BTC-DTG-1.52 (DTG = dithioglycol), respectively, in the present work.

2.3. Mercury adsorption studies

The capacity of the thiol-modified $[Cu_3(BTC)_2]_n$ samples to adsorb mercury ion from water was determined using a batch of mercury chloride aqueous solutions of known concentration. 10 mg of the thiol-functionalized $[Cu_3(BTC)_2]_n$ crystals were added to 10 mL of the Hg^{2+} solutions (1431.04, 1252.16, 1073.28, 894.40, 715.52, 143.10, 6.51, 1.30, 0.65, 0.16 and 0.08 mg L^{-1}, respectively) under constant shaking at room temperature for 24 h. After high-speed centrifugation, both initial and the remaining Hg^{2+} concentrations were determined with AFS.

3. Results and discussion

3.1. Characterization

3.1.1. PXRD measurements

The synthesis of the dithioglycol grafted $[Cu_3(BTC)_2]_n$ through coordination of dithioglycol to the unsaturated metal centers of the dehydrated $[Cu_3(BTC)_2]_n$ framework was performed in anhydrous toluene under magnetic stirring at room temperature. Initial evidence of the as-synthesized thiol-functionalized samples was confirmed by PXRD (Fig. 2). All of the diffraction peaks for thiol-functionalized samples **A** and **B** show that the sketch of the MOF $[Cu_3(BTC)_2]_n$ crystal is well retained even after the modification with dithioglycol, because all diffraction peaks of the functionalized $[Cu_3(BTC)_2]_n$ can readily be indexed to HKUST-1. For sample **C**, however, modification of $[Cu_3(BTC)_2]_n$ with excessive dithioglycol resulted in loss of crystalline order of the framework, as evidenced by significant decrease in diffraction intensities (see Fig. 2d), which is due to partial decomposition of the crystalline $[Cu_3(BTC)_2]_n$.

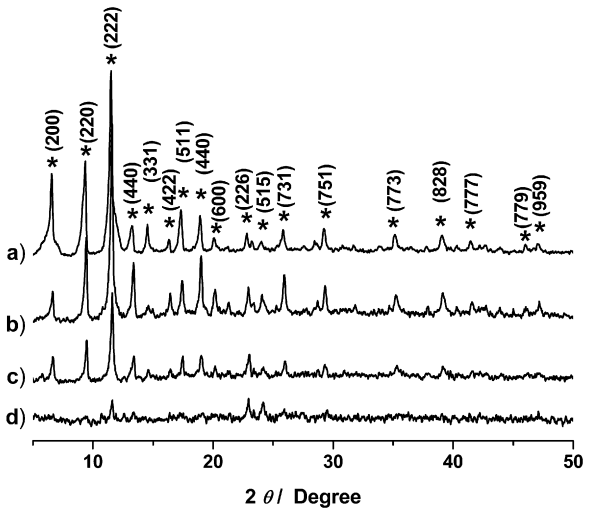

Fig. 2. PXRD patterns of (a) as-synthesized $[Cu_3(BTC)_2(H_2O)_3]_n$ crystals, and (b–d) thiol-modified $[Cu_3(BTC)_2]_n$ samples **A** (Cu-BTC-DTG-0.18), **B** (Cu-BTC-DTG-0.92), and **C** (Cu-BTC-DTG-1.52), respectively.

3.1.2. SEM–EDX measurements

To interrogate the surface morphology and chemical composition of the functionalized samples, the thiol-functionalized samples were characterized by SEM (Fig. 3) and EDX (Fig. 4). The crystals of original $[Cu_3(BTC)_2]_n$ sample before the thiol-functionalization are octahedral with a smooth surface and have an average size of 8 μm (Fig. 3a). However, surfaces of the thiol-modified $[Cu_3(BTC)_2]_n$ samples **A**, **B** and **C** tend to be rougher after the functionalization (Fig. 3b–d). Moreover, for the thiol-modified sample **C**, increasing S/Cu molar ratio to 1.52 caused a significant morphological change from regular octahedral $[Cu_3(BTC)_2]_n$ crystals to irregular particles, which is due to partial decomposition of the framework. The EDX spectra of the thiol-functionalized samples reveal that the samples

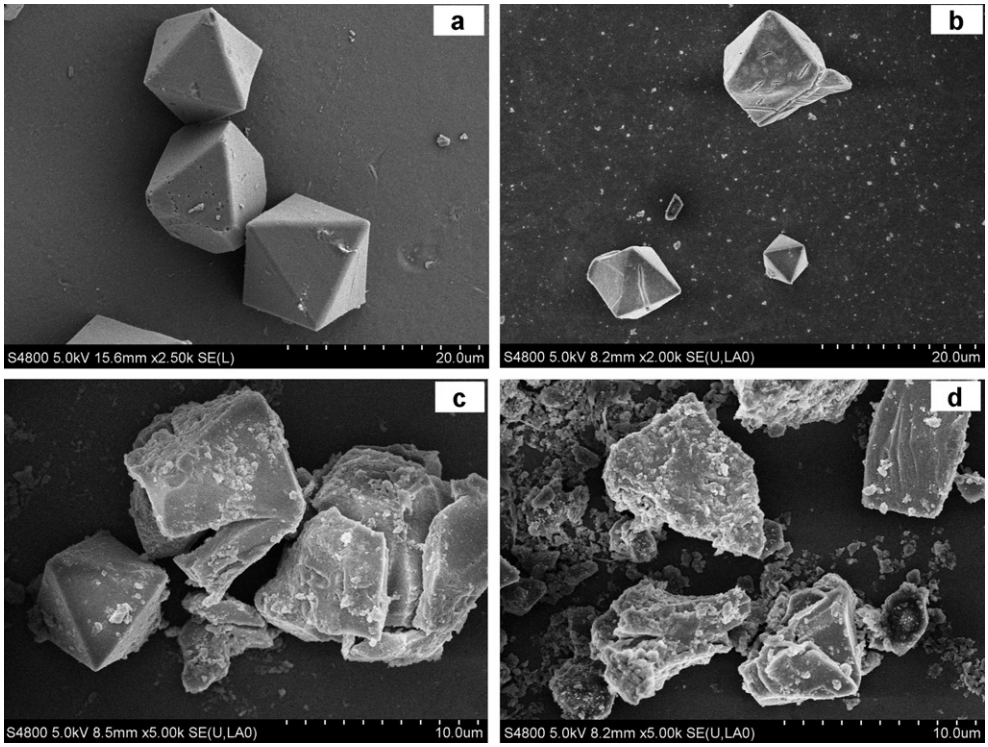

Fig. 3. SEM images of (a) the as-synthesized $[Cu_3(BTC)_2(H_2O)_3]_n$, and (b–d) the thiol-modified $[Cu_3(BTC)_2]_n$ samples **A** (Cu-BTC-DTG-0.18), **B** (Cu-BTC-DTG-0.92), and **C** (Cu-BTC-DTG-1.52), respectively.

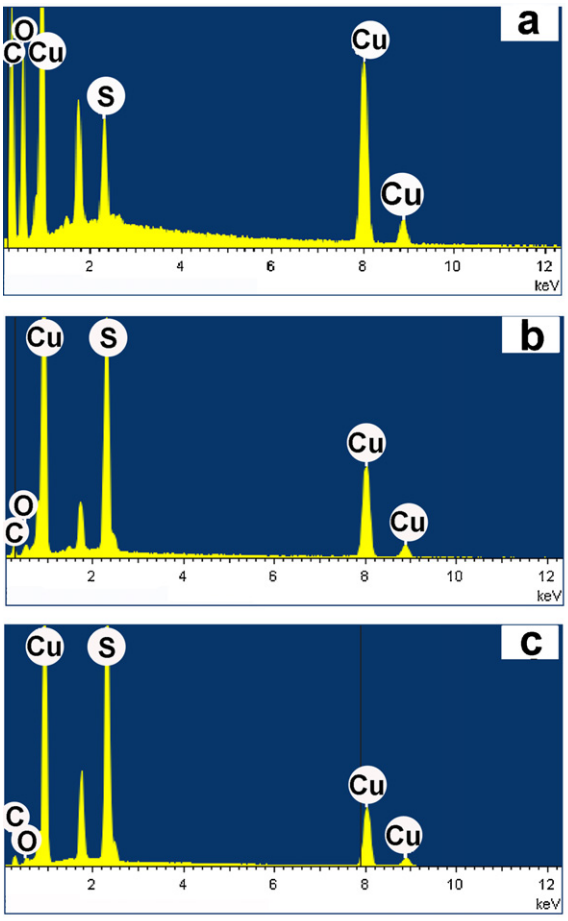

Element	Mass-%	Atom-%
C K	42.53	63.00
O K	24.21	26.92
S K	2.77	1.54
Cu K	30.49	8.54
Total	100.00	

Element	Mass-%	Atom-%
C K	19.95	48.32
O K	2.95	5.37
S K	24.51	22.24
Cu K	52.59	24.08
Total	100.00	

Element	Mass-%	Atom-%
C K	21.06	48.61
O K	2.03	3.52
S K	33.37	28.86
Cu K	43.54	19.00
Total	100.00	

Fig. 4. EDX spectra of (a–c) the thiol-modified $[Cu_3(BTC)_2]_n$ samples **A** (Cu-BTC-DTG-0.18), **B** (Cu-BTC-DTG-0.92), and **C** (Cu-BTC-DTG-1.52), respectively.

are composed of C, O, Cu and S, as shown in Fig. 4a–c. The relative contents of S in the functionalized samples **A**, **B** and **C** were determined to be 0.83, 4.24 and 6.98 mmol g^{-1} of $[Cu_3(BTC)_2]_n$, which correspond to S/Cu ratio of 0.18, 0.92, 1.52, respectively (Table 1), suggesting that content of –SH group grafted on the framework can easily be tuned by varying molar ratio of dithioglycol to the framework.

3.1.3. IR measurement

Fig. 5 shows IR spectra of the thiol-functionalized samples, as well as the bare $[Cu_3(BTC)_2(H_2O)_3]_n$ crystals. The bare $[Cu_3(BTC)_2(H_2O)_3]_n$ shows bands ν(ArC–H) corresponding to aromatic groups at 3050 cm^{-1}, and vibrational bands characteristics of the –O–C–O– group around 1550 and 1430 cm^{-1} (Fig. 5a). The bands around 2900, 2581, and 686 cm^{-1} observed in thiol-functionalized samples can be attributed to the presence of ν(C–H), ν(S–H), and ν(C–S) vibrations, respectively (see Fig. 5b–d), indicating the presence of dithioglycol. Although the peak at 2581 cm^{-1} corresponding to ν(S–H) is not very strong, obvious shift of the aliphatic ν(C–H) stretching vibrations at 2800–3000 cm^{-1} to larger values was found, as observed when the molecule is coordinated to a Lewis acid center [30,33]. The result clearly reveals that dithioglycol molecules were successfully grated onto the UMCs in channels created in the framework, rather than adsorbed on external surface of $[Cu_3(BTC)_2]_n$ crystals. This result was also confirmed by N_2 sorption–desorption isotherms of the samples as shown below.

3.1.4. N_2 sorption–desorption isotherms

The resulting of thiol-grafting on coordinatively unsaturated copper centers of $[Cu_3(BTC)_2]_n$ crystal is also visible in the N_2 sorption–desorption isotherms. The N_2 sorption–desorption isotherms of the as-synthesized samples reveal a typical microporous material (Fig. 6). Compared with the pristine

Table 1
Physicochemical properties of $[Cu_3(BTC)_2(H_2O)_3]_n$ and its dithioglycol-functionalized analogs.

Sample	S_{BET}[a] ($m^2\ g^{-1}$)	V_t[b] ($m^3\ g^{-1}$)	S content[c] (mmol g^{-1})	S/Cu ratio	K_d(Hg)[d] (mL g^{-1})
$[Cu_3(BTC)_2(H_2O)_3]_n$	1492.19	0.75	–	–	0
A (Cu-BTC-DTG-0.18)	800.42	0.38	0.83	0.18	
B (Cu-BTC-DTG-0.92)	331.39	0.18	4.24	0.92	4.73×10^5
C (Cu-BTC-DTG-1.52)	79.92	0.05	6.98	1.52	

[a] S_{BET} represents BET surface areas obtained from N_2 sorption–desorption isotherms.
[b] V_t represents pore volumes obtained from N_2 sorption–desorption isotherms.
[c] S content represents the relative contents of S in the functionalized samples per gram of $[Cu_3(BTC)_2]_n$.
[d] K_d(Hg) represents the distribution coefficient of Hg^{2+} ion.

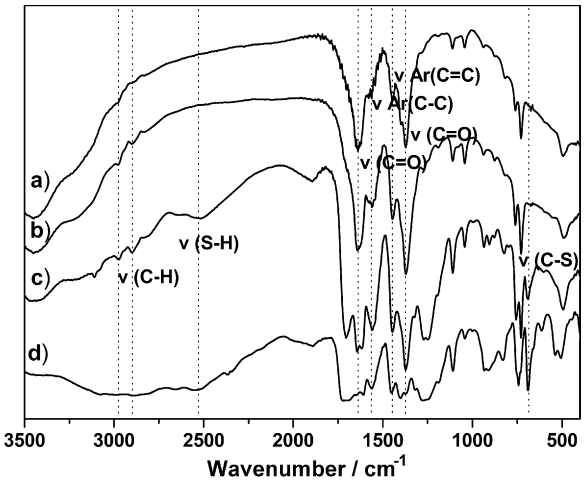

Fig. 5. Infrared spectra of (a) the as-synthesized $[Cu_3(BTC)_2(H_2O)_3]_n$, and (b–d) the thiol-modified $[Cu_3(BTC)_2]_n$ samples **A** (Cu-BTC-DTG-0.18), **B** (Cu-BTC-DTG-0.92), and **C** (Cu-BTC-DTG-1.52), respectively.

$[Cu_3(BTC)_2(H_2O)_3]_n$, the thiol-modificated samples exhibit a significant decrease in both surface areas and pore volumes. The Brunauer–Emmett–Teller surface areas (S_{BET}) of the thiol-functionalized samples **A**, **B**, and **C** decreased significantly from 1492.19 $m^2\,g^{-1}$ to 800.42, 331.39 and 79.92 $m^2\,g^{-1}$, and pore volumes (V_t) decreased from 0.75 $cm^3\,g^{-1}$ to 0.38, 0.18 and 0.05 $cm^3\,g^{-1}$, respectively, after dithioglycol-grafting (Table 1). The result indicates that the pores of the $[Cu_3(BTC)_2]_n$ are partially blocked after the thiol-grafting, leaving limited accessible pore volume for nitrogen molecules. The occupation of partial space in the channels of the $[Cu_3(BTC)_2]_n$ sample by dithioglycol molecules resulted in a significant decrease in both surface area and pore volume of the thiol-functionlized $[Cu_3(BTC)_2]_n$ samples, clearly demonstrating that the grafted thiol groups are present in the channels of $[Cu_3(BTC)_2]_n$ rather than on the surfaces of the $[Cu_3(BTC)_2]_n$ crystals as discussed above.

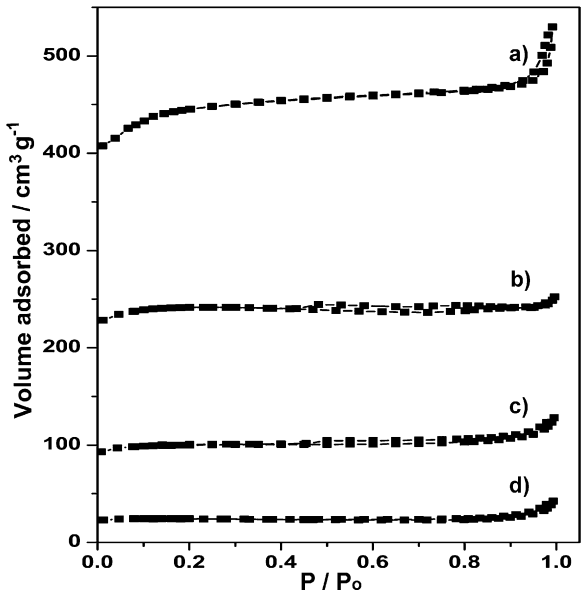

Fig. 6. Nitrogen sorption–desorption isotherms of (a) the as-synthesized $[Cu_3(BTC)_2(H_2O)_3]_n$, and (b–d) the thiol-modified $[Cu_3(BTC)_2]_n$ samples **A** (Cu-BTC-DTG-0.18), **B** (Cu-BTC-DTG-0.92), and **C** (Cu-BTC-DTG-1.52), respectively.

Table 2
Hg^{2+} concentrations in aqueous solutions before and after treating with the thiol-modified $[Cu_3(BTC)_2]_n$ sample **B** (Cu-BTC-DTG-0.92).[a]

Hg^{2+} concentration ($mg\,L^{-1}$)		Adsorption capacity ($mg\,g^{-1}$)	Removal efficiency (%)
Initial	After adsorption		
1431.04	712.90	718.14	50.18
1252.16	542.67	709.49	56.67
1073.28	388.75	684.53	63.78
894.40	179.63	714.78	79.92
715.52	1.51	714.01	99.79
143.10	0.13	142.96	99.91
6.51	0.011	6.50	99.83
1.30	0.015	1.29	98.85
0.65	0.019	0.63	97.07
0.16	0.0074	0.16	95.38
0.081	0.0075	0.074	90.74

[a] Adsorption conditions: 10 mg of the thiol-functionalized $[Cu_3(BTC)_2]_n$ crystals were added to 10 mL of the Hg^{2+} solutions under constant shaking at room temperature for 24 h. After high-speed centrifugation, both initial and the remaining Hg^{2+} concentrations were determined with AFS.

3.2. Adsorption isotherms for Hg^{2+} removal from water

The ability of such thiol-functionalized MOFs to remove heavy metal ions from contaminated water was preliminarily demonstrated by removal of mercury ion from water using the thiol-functionlized $[Cu_3(BTC)_2]_n$ sample **B** under a wide range of known mercury concentrations. As shown in Table 2, the treatment of Hg^{2+} solution with sample **B** resulted in 99.79% removal of Hg^{2+} ion with an unprecedented adsorption capacity of 714.01 $mg\,g^{-1}$ when initial Hg^{2+} concentration was as high as 715.5 $mg\,L^{-1}$. More importantly, the sample could still remove 90.74% of Hg^{2+} ion from the solution even when initial Hg^{2+} concentration was as low as 81 ppb. Adsorption of Hg^{2+} from aqueous solution using bare $[Cu_3(BTC)_2(H_2O)_3]_n$ sample was also carried out as a control experiment, and no detectable amount of Hg^{2+} ion was adsorbed by the unfunctionalized $[Cu_3(BTC)_2(H_2O)_3]_n$. In addition, compared with other functionalized porous adsorbents such as ion-exchange resin and hybrid silica materials, the thiol-functionalized MOF exhibits a significantly high adsorption capacity [6,11]. Such high capacity of the thiol-functionalized MOFs for Hg^{2+} adsorption can be attributed to the thiol groups densely populated on the inner surface of porous MOFs with unique large specific surface areas and high density of adsorption sites.

To gain a better understanding of the mechanism of the heavy metal removal, the thiol-functionalized sample was characterized using the adsorption isotherm. Fig. 7 shows the adsorption isotherm of Hg^{2+} onto the thiol-functionalized MOF sample **B**. Remarkably, the equilibrium adsorption capacities of Hg^{2+} increase sharply with an increase in Hg^{2+} initial concentration when its value is lower than 715.52 $mg\,L^{-1}$. However, when concentration of Hg^{2+} ion is higher than this value, increasing the Hg^{2+} concentration does not affect adsorption capacity of Hg^{2+}, which is due to saturated adsorption of Hg^{2+} onto the thiol-functionalized sample.

By fitting the equilibrium adsorption data with Langmuir adsorption model, adsorption capacity of Hg^{2+} onto the thiol-functionalized sample was calculated from Eq. (1) [34,35]:

$$\frac{C_e}{q_e} = \frac{1}{q_m K_L} + \frac{C_e}{q_m} \quad (1)$$

where C_e is the equilibrium concentration of remaining Hg^{2+} ion in the solution ($mg\,L^{-1}$), q_e is the amount of Hg^{2+} ion adsorbed per mass unit of adsorbent at equilibrium ($mg\,g^{-1}$), q_m is the monolayer adsorption capacity ($mg\,g^{-1}$), and K_L is the Langmuir constant ($L\,mg^{-1}$).

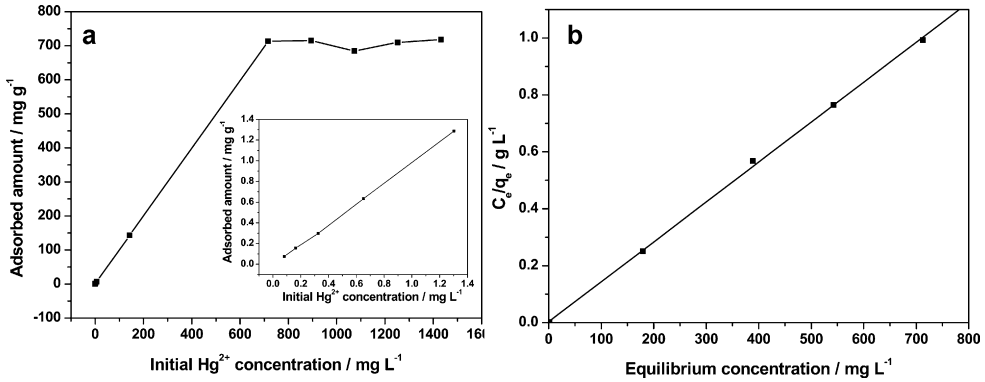

Fig. 7. (a) Adsorption curve of Hg^{2+} at different concentrations by using the thiol-modified $[Cu_3(BTC)_2]_n$ samples **B** (Cu-BTC-DTG-0.92); inset shows adsorption curve of Hg^{2+} at low concentrations. (b) The linear regression by fitting the equilibrium adsorption data with Langmuir adsorption model.

The linear regression between C_e/q_e and C_e was calculated, and the correlation coefficient of the straight line is 0.9997, indicating that the adsorption of Hg^{2+} ion conforms Langmuir's adsorption model. Remarkably, the maximum adsorption capacity of the thiol-functionalized $[Cu_3(BTC)_2]_n$ sample was calculated to be 714.29 mg g^{-1} for Hg^{2+}, which corresponds to capture of 0.952 Hg^{2+} ion per terminal thiol group in the thiol-functionalized $[Cu_3(BTC)_2]_n$, suggesting that Hg^{2+} ion were allowed to access almost all free thiol groups in the functionalized $[Cu_3(BTC)_2]_n$. The maximum adsorption capacity value is higher than many other conventional porous adsorbents [34,35].

The ability of the thiol-functionalized MOF to remove Hg^{2+} ion from water can be also expressed with a distribution coefficient (K_d), which is defined as the following equation [36]

$$K_d = \frac{(C_i - C_f)}{C_f} \times \frac{V}{m} \quad (2)$$

where C_i and C_f represent the initial and final solution concentrations, respectively, V represents the volume of solution (mL), and m represents the mass of adsorbent (g). The K_d value of the thiol-functionalized sample **B** for Hg^{2+} adsorption is listed in Table 1. Although bare $[Cu_3(BTC)_2(H_2O)_3]_n$ has no binding affinity to Hg^{2+}, the thiol-functionalization of $[Cu_3(BTC)_2(H_2O)_3]_n$ leads to a significant increase in the binding capacity for Hg^{2+}. The K_d value for the thiol functionalized sample **B** was calculated to be 4.73×10^5 mL g^{-1} for Hg^{2+} in the single solution, which is higher than some functionalized nanoporous silica reported very recently [36].

Although a few of MOFs and zeolitic imidazolate frameworks (ZIFs), such as MIL-101 and ZIF-8, exhibit exceptional chemical stability, many other organic–inorganic hybrid materials are commonly unstable under strong acidic conditions. As a result, it may be a challenge to recycle such MOF-type absorbents after heavy metal adsorption because efficient regeneration of the absorbents (e.g. activated carbon, ion-exchange resin, and thiol-functionalized mesoporous silica) after heavy metal adsorption has always to be carried out under strong acidic conditions. However, the present work establishes a simple and efficient route to a novel type of thiol-functionalized adsorbents for heavy metal removal on the basis of MOFs-based materials. Such the thiol-functionalized MOFs exhibit remarkably high adsorption capacity for heavy metal removal, as clearly demonstrated in the present work. In addition, high removal efficiencies were also observed for heavy metal removal from water; removal percent varied from 95.38 to 99.79% depending on various Hg^{2+} concentrations. More importantly, such absorbent exhibits a significantly high efficiency for Hg^{2+} removal even when concentration of heavy metal ion is extremely low (81 ppb). Very recently, we reported a facile and environmentally friendly fabrication of a novel type of magnetic porous MOF-based nanocomposites by incorporation of Fe_3O_4 nanorods with MOF nanocrystals. Such MOF-based nanocomposites exhibited both magnetic characteristics and high porosity [19]. These properties may provide the thiol-functionalized MOFs more chances in biomedical applications (for example, decorporation of metal toxins from biological environment and targeted drug delivery).

3.3. Adsorption kinetics

In order to evaluate the kinetic mechanism that controls the adsorption process, the effect of contact time on the adsorption of Hg^{2+} onto the thiol-functionalized $[Cu_3(BTC)_2]_n$ was further investigated by adding 10 mg of sample **B** to 10 mL of 6.51 mg L^{-1} Hg^{2+} solution. As can be seen in Fig. 8, the thiol-functionalized sample attained 99% of the adsorption capacity at equilibrium within 120 min, suggesting that the thiol-functionalized MOF possesses both a high adsorption capacity and a high adsorption efficiency for the removal of heavy metal ions from water.

The rate constant for pseudo-second-order adsorption could be obtained from the following equation [37,38]:

$$\frac{t}{q_t} = \frac{1}{k_2 q_e^2} + \frac{t}{q_e} \quad (3)$$

where k_2 is the rate constant of the pseudo-second-order adsorption (g mg^{-1} min^{-1}), and q_t is the amount of Hg^{2+} adsorbed at time t

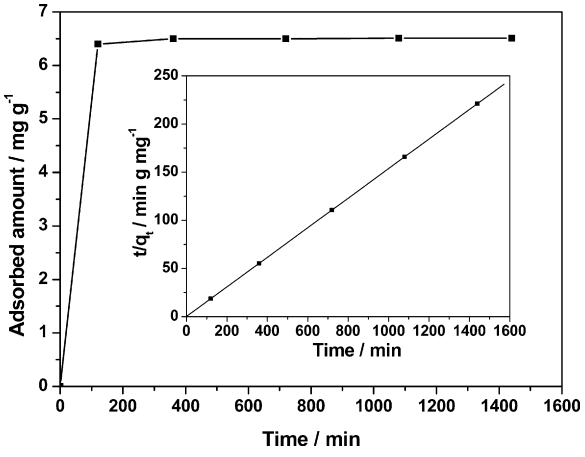

Fig. 8. Adsorption curve of Hg^{2+} versus contact time in aqueous solution by using the thiol-modified $[Cu_3(BTC)_2]_n$ samples **B** (Cu-BTC-DTG-0.92). Inset shows the pseudo-second-order kinetic plot for the adsorption (Hg^{2+} concentration: 6.51 mg L^{-1}).

($mg\,g^{-1}$). By fitting the experimental date with the pseudo-second-order kinetic model using Eq. (3), the adsorption rate constant k_2, the calculated q_e value and the correlation coefficient were obtained. An extremely high correlation coefficient (0.9999) was obtained. Moreover, the calculated q_e value also agrees with the experimental data in the case of pseudo-second-order kinetics, suggesting the adsorption of Hg^{2+} onto the adsorbent follows a pseudo-second-order kinetic model. The value of the adsorption rate constant k_2 under this condition in the present work was determined to be $0.13\,g\,mg^{-1}\,min^{-1}$. This value exceeds many other porous absorbents [34,35,37,38], which can also be attributed to the thiol groups densely populated on the inner surface of porous MOFs with unique large specific surface areas and high density of adsorption sites.

4. Conclusions

In conclusion, the present work demonstrates a facile strategy to fabricate thiol-functionalized porous MOFs as a novel type of adsorbent for removal of Hg^{2+}. Thiol-functionalized $[Cu_3(BTC)_2]_n$ samples with different S/Cu molar ratio were prepared by thiol grafting on coordinatively unsaturated copper center in a 3D porous MOF, $[Cu_3(BTC)_2]_n$, and their structures, morphologies and porosity were characterized. Although the unfunctionalized $[Cu_3(BTC)_2]_n$ showed no adsorption of Hg^{2+}, the thiol-functionalized samples exhibited a high affinity (distribution coefficient $K_d = 4.73 \times 10^5\,mL\,g^{-1}$) and significant adsorption capacity ($714.29\,mg\,g^{-1}$) for Hg^{2+} removal from aqueous solution, making them potential for selective removal of heavy metal ions from water. We believe that this work establishes a simple and energy efficient route to a novel type of adsorbents for heavy metal removal on the basis of the functionalization of MOFs-based materials. Also, the present strategy for tailoring MOFs-based porous materials by grafting different organic functional groups using coordination chemistry will offer a plethora of opportunities for generating new functionalized materials for dye adsorption, CO_2 capture, sensing, as well as gas purification.

Acknowledgments

This work was supported by the National Natural Science Foundation of China (NSFC, 20971001), the NSFC-CAS Joint Fund for Research Based on Large-Scale Scientific Facilities (10979014), the Program for New Century Excellent Talent in University, Ministry of Education, China (NCET-08-0617), and the "211 Project" of Anhui University. J.-F. Zhu is grateful for the financial support from NSFC (20873128) and the "Hundred Talents Program" of the Chinese Academy of Sciences.

References

[1] C. Wang, S.Y. Tao, W. Wei, C.G. Meng, F.Y. Liu, M. Han, Multifunctional mesoporous material for detection, adsorption and removal of Hg^{2+} in aqueous solution, J. Mater. Chem. 20 (2010) 4635–4641.
[2] P. Miretzky, A.F. Cirelli, Hg(II) removal from water by chitosan and chitosan derivatives: a review, J. Hazard. Mater. 167 (2009) 10–23.
[3] W.S. Wan Ngah, M.A.K.M. Hanafiah, Removal of heavy metal ions from wastewater by chemically modified plant wastes as adsorbents: a review, Bioresour. Technol. 99 (2008) 3935–3948.
[4] V.K. Gupta, P.J.M. Carrott, M.M.L. Ribeiro Carrott, Suhas, Low-cost adsorbents: growing approach to wastewater treatment—a review, Crit. Rev. Environ. Sci. Technol. 39 (2009) 783–842.
[5] P. Kumar, V.V. Guliants, Periodic mesoporous organic–inorganic hybrid materials: applications in membrane separations and adsorption, Micropor. Mesopor. Mater. 132 (2010) 1–14.
[6] A. Dąbrowski, Z. Hubicki, P. Podkościelny, E. Robens, Selective removal of the heavy metal ions from waters and industrial wastewaters by ion-exchange method, Chemosphere 56 (2004) 91–106.
[7] M. Huebra, M.P. Elizalde, A. Almela, Hg(II) extraction by LIX 34. Mercury removal from sludge, Hydrometallurgy 68 (2003) 33–42.
[8] D. Mohan, C.U. Pittman Jr., Activated carbons and low cost adsorbents for remediation of tri- and hexavalent chromium from water, J. Hazard. Mater. 137 (2006) 762–811.
[9] S.B. Wang, Y.L. Peng, Natural zeolites as effective adsorbents in water and wastewater treatment, Chem. Eng. J. 156 (2010) 11–24.
[10] K.G. Bhattacharyya, S.S. Gupta, Adsorption of a few heavy metals on natural and modified kaolinite and montmotillonite: a review, Adv. Colloid Interface Sci. 140 (2008) 114–131.
[11] K.S. Xia, R.Z. Ferguson, M. Losier, N. Tchoukanova, R. Brüning, Y. Djaoued, Synthesis of hybrid silica materials with tunable pore structures and morphology and their application for heavy metal removal from drinking water, J. Hazard. Mater. 183 (2010) 554–564.
[12] G. Férey, Hybrid porous solids: past, present, future, Chem. Soc. Rev. 37 (2008) 191–214.
[13] J.Y. Lee, O.K. Farha, J. Roberts, K.A. Scheidt, S.T. Nguyen, J.T. Hupp, Metal-organic framework materials as catalysts, Chem. Soc. Rev. 38 (2009) 1450–1459.
[14] A. Corma, H. García, F.X. Llabrés i Xamena, Engineering metal organic frameworks for heterogeneous catalysis, Chem. Rev. 110 (2010) 4606–4655.
[15] J.W. Yoon, S.H. Jhung, Y.K. Hwang, S.M. Humphrey, P.T. Wood, J.-S. Chang, Gas-sorption selectivity of CUK-1: a porous coordination solid made of cobalt(II) and pyridine-2,4-dicarboxylic acid, Adv. Mater. 19 (2007) 1830–1834.
[16] P. Horcajada, C. Serre, M. Vallet-Regí, M. Sebban, F. Taulelle, G. Férey, Metal-organic frameworks as efficient materials for drug delivery, Angew. Chem. Int. Ed. 45 (2006) 5974–5978.
[17] K.M.L. Taylor-Pashow, J.D. Rocca, Z.G. Xie, S. Tran, W.B. Lin, Postsynthetic modifications of iron-carboxylate nanoscale metal-organic frameworks for imaging and drug delivery, J. Am. Chem. Soc. 131 (2009) 14261–14263.
[18] P. Horcajada, T. Chalati, C. Serre, B. Gillet, C. Sebrie, T. Baati, J.F. Eubank, D. Heurtaux, P. Clayette, C. Kreuz, J.-S. Chang, Y.K. Hwang, V. Marsaud, P.-N. Bories, L. Cynober, S. Gil, G. Férey, P. Couvreur, R. Gref, Porous metal-organic-framework nanoscale carriers as a potential platform for drug delivery and imaging, Nat. Mater. 9 (2010) 172–178.
[19] F. Ke, Y.P. Yuan, L.G. Qiu, Y.H. Shen, A.J. Xie, J.F. Zhu, X.Y. Tian, L.D. Zhang, Facile fabrication of magnetic metal-organic framework nanocomposites for potential targeted drug delivery, J. Mater. Chem. 21 (2011) 3843–3848.
[20] Y.H. Hu, L. Zhang, Hydrogen storage in metal-organic frameworks, Adv. Mater. 22 (2010) E117–E130.
[21] L.G. Qiu, Z.Q. Li, Y. Wu, W. Wang, T. Xu, X. Jiang, Facile synthesis of nanocrystals of a microporous metal-organic framework by an ultrasonic method and selective sensing of organoamines, Chem. Commun. 364 (2008) 2–3644.
[22] K. Koh, A.G. Wong-Foy, A.J. Matzger, A porous coordination copolymer with over $5000\,m^2/g$ BET surface area, J. Am. Chem. Soc. 131 (2009) 4184–4185.
[23] Z.Q. Wang, S.M. Cohen, Postsynthetic modification of metal-organic frameworks, Chem. Soc. Rev. 38 (2009) 1315–1329.
[24] J.L.C. Rowsell, O.M. Yaghi, Effects of functionalization, catenation, and variation of the metal oxide and organic linking units on the low-pressure hydrogen adsorption properties of metal-organic frameworks, J. Am. Chem. Soc. 128 (2006) 1304–1315.
[25] Y. Liu, G. Li, X. Li, Y. Cui, Cation-dependent nonlinear optical behavior in an octupolar 3D anionic metal-organic open framework, Angew. Chem. Int. Ed. 46 (2007) 6301–6304.
[26] Z.Q. Wang, S.M. Cohen, Postsynthetic covalent modification of a neutral metal-organic framework, J. Am. Chem. Soc. 129 (2007) 12368–12369.
[27] J.G. Nguyen, S.M. Cohen, Moisture-resistant and superhydrophobic metal-organic frameworks obtained via postsynthetic modification, J. Am. Chem. Soc. 132 (2010) 4560–4561.
[28] S. Kitagawa, S.-I. Noro, T. Nakamura, Pore surface engineering of microporous coordination polymers, Chem. Commun. 70 (2006) 1–707.
[29] S. Hasegawa, S. Horike, R. Matsuda, S. Furukawa, K. Mochizuki, Y. Kinoshita, S. Kitaggawa, Three-dimensional porous coordination polymer functionalized with amide groups based on tridentate ligand: selective sorption and catalysis, J. Am. Chem. Soc. 129 (2007) 2607–2614.
[30] Y.K. Hwang, D.-Y. Hong, J.-S. Chang, S.H. Jhung, Y.-K. Seo, J. Kim, A. Vimont, M. Daturi, C. Serre, G. Férey, Amine grafting on coordinatively unsaturated metal centers of MOFs: consequences for catalysis and metal encapsulation, Angew. Chem. Int. Ed. 47 (2008) 4144–4148.
[31] E. Haque, J.E. Lee, I.T. Jang, Y.K. Hwang, J.-S. Chang, J. Jegal, S.H. Jhung, Adsorptive removal of methyl orange from aqueous solution with metal-organic frameworks, porous chromium-benzenedicarboxylates, J. Hazard. Mater. 181 (2010) 535–542.
[32] S.S.-Y. Chui, S.M.-F. Lo, J.P.H. Charmant, A.G. Orpen, I.D. Williams, A chemically functionalizable nanoporous material $[Cu_3(TMA)_2(H_2O)_3]_n$, Science 283 (1999) 1148–1150.
[33] K. Nakamoto, Infrared and Raman Spectra of Inorganic and Coordination Compounds, 6th ed., John Wiley & Sons Inc., Hoboken, New Jersey, 2009.
[34] C.M. Sun, F. Ma, G.H. Zhang, R.J. Qu, Y. Zhang, Removal of mercury ions from ethanol solution using silica gel functionalized with amino-terminated dendrimer-like polyamidoamine polymers: kinetics and equilibrium studies, J. Chem. Eng. Data, in press.
[35] R.J. Qu, M.H. Wang, R.F. Song, C.M. Sun, Y. Zhang, X.Y. Sun, C.N. Ji, C.H. Wang, P. Yin, Adsorption kinetics and isotherms of Ag(I) and Hg(II) onto silica gel with functional groups of hydroxyl- or amino-terminated polyamines, J. Chem. Eng. Data 56 (2011) 1982–1990.

[36] W. Yantasee, R.D. Rutledge, W. Chouyyok, V. Sukwarotwat, G. Orr, C.L. Warner, M.G. Warner, G.E. Fryxell, R.J. Wiacek, C. Timchalk, R.S. Addleman, Functionalized nanoporous silica for the removal of heavy metals from biological systems: adsorption and application, ACS Appl. Mater. Interfaces 2 (2010) 2749–2758.
[37] R.J. Qu, Y. Zhang, C.M. Sun, C.H. Wang, C.N. Ji, H. Chen, P. Yin, Adsorption of Hg(II) from an aqueous solution by silica-gel supported diethylenetriamine prepared via different routes: kinetics, thermodynamics and isotherms, J. Chem. Eng. Data 55 (2010) 1496–1504.
[38] R. Rostamian, M. Najafi, A.A. Rafati, Synthesis and characterization of thiol-functionalized silica nano hollow sphere as a novel adsorbent for removal of poisonous heavy metal ions from water: kinetics isotherms and error analysis, Chem. Eng. J. 171 (2011) 1004–1011.